Calcium oxalate crystals induce renal inflammation by NLRP3-mediated IL-1β secretion

Shrikant R. Mulay,[1] Onkar P. Kulkarni,[1] Khader V. Rupanagudi,[1] Adriana Migliorini,[1] Murthy N. Darisipudi,[1] Akosua Vilaysane,[2] Daniel Muruve,[2] Yan Shi,[3] Fay Munro,[3] Helen Liapis,[4] and Hans-Joachim Anders[1]

[1]Nephrologisches Zentrum, Medizinische Klinik und Poliklinik IV, Klinikum der Universität München, Munich, Germany. [2]Department of Medicine, Division of Nephrology and Hypertension, Department of Medicine and the Immunology Research Group, Institute of Infection, Immunity and Inflammation, and [3]Department of Medicine, Department of Microbiology, Immunology and Infectious Diseases, University of Calgary, Calgary, Alberta, Canada. [4]Department of Pathology and Immunology, Washington University School of Medicine, Saint Louis, Missouri, USA.

Nephrocalcinosis, acute calcium oxalate (CaOx) nephropathy, and renal stone disease can lead to inflammation and subsequent renal failure, but the underlying pathological mechanisms remain elusive. Other crystallopathies, such as gout, atherosclerosis, and asbestosis, trigger inflammation and tissue remodeling by inducing IL-1β secretion, leading us to hypothesize that CaOx crystals may induce inflammation in a similar manner. In mice, intrarenal CaOx deposition induced tubular damage, cytokine expression, neutrophil recruitment, and renal failure. We found that CaOx crystals activated murine renal DCs to secrete IL-1β through a pathway that included NLRP3, ASC, and caspase-1. Despite a similar amount of crystal deposits, intrarenal inflammation, tubular damage, and renal dysfunction were abrogated in mice deficient in MyD88; NLRP3, ASC, and caspase-1; IL-1R; or IL-18. Nephropathy was attenuated by DC depletion, ATP depletion, or therapeutic IL-1 antagonism. These data demonstrated that CaOx crystals trigger IL-1β–dependent innate immunity via the NLRP3/ASC/caspase-1 axis in intrarenal mononuclear phagocytes and directly damage tubular cells, leading to the release of the NLRP3 agonist ATP. Furthermore, these results suggest that IL-1β blockade may prevent renal damage in nephrocalcinosis.

Introduction

Kidney stone disease affects about 12% of men and 5% of women during their lifetimes in the United States (1). Unlike symptomatic urolithiasis, intrarenal nephrocalcinosis is often asymptomatic, but can lead to significant kidney injury and renal failure (1–3). Calcium oxalate (CaOx) stones account for the vast majority of calculi in primary and secondary forms of hyperoxaluria (4, 5). In addition, acute oxalosis (e.g., in ethylene glycol poisoning) can induce acute kidney injury as a result of widespread intrarenal CaOx deposition (6). Histopathology of human CaOx nephropathy as well as microarray analysis of rodent CaOx nephropathy document a substantial contribution of interstitial inflammation to tissue remodeling, but the molecular and cellular mechanisms of CaOx-induced renal inflammation remain largely unknown (7–11).

Inflammation and tissue remodeling in various crystallopathies, such as gout (caused by monosodium urate crystals), pseudogout (caused by calcium pyrophosphate crystals; ref. 12); atherosclerosis (caused by cholesterol crystals; ref. 13) silicosis (caused by silica crystals; ref. 14) and asbestosis (caused by asbestos; ref. 14), involve a unique intracellular signaling pathway for the secretion of the proinflammatory cytokine IL-1β: the NLRP3 inflammasome/apoptosis-associated speck-like protein containing CARD/caspase-1 (NLRP3/ASC/caspase-1) axis (15). The NLRP3 inflammasome is a large cytoplasmatic protein complex able to integrate multiple extracellular and intracellular danger signals into ASC binding and activation of caspase-1 (also known as pro–IL-1β converting enzyme; ref. 15). In contrast to other NF-κB–dependent cytokines that are readily secreted, the inactive pro-form of IL-1β requires cleavage (e.g., by caspase-1) as an additional enzymatic step before the bioactive form of IL-1β can be secreted from the cell (15).

Here, we hypothesized that CaOx crystals have a similar agonistic potential on NLRP3 and trigger IL-1β secretion and that this process contributes to CaOx-induced tissue inflammation, for example, in nephrocalcinosis and/or CaOx nephropathy.

Results

CaOx crystals need NLRP3/ASC/caspase-1 to induce IL-1β in DCs. We hypothesized that CaOx crystals have the same potential to activate DCs as do crystals of uric acid, calcium pyrophosphate, or cholesterol (12, 13). CaOx crystals were of small size when used in vitro together with bone marrow–derived DCs (BMDCs; Supplemental Figure 1; supplemental material available online with this article; doi:10.1172/JCI63679DS1). CaOx crystal exposure activated murine BMDCs to release IL-1β in a dose-dependent manner, but only when cells were prestimulated with LPS, TNF, IL-1α, or histones (Figure 1A and Supplemental Figure 2). Western blotting of DC supernatants revealed that LPS prestimulation was a prerequisite for induction of pro–IL-1β expression (Figure 1A). LPS also induced pro–caspase-1 in BMDCs, and CaOx crystals induced caspase-1 activation similar to that by the NLRP3 agonist ATP (Figure 1A). To address a potential NLRP3 agonistic effect of CaOx crystals, BMDCs from *Nlrp3*$^{-/-}$, *Asc*$^{-/-}$, and *Casp1*$^{-/-}$ mice were also prepared; LPS/CaOx crystals were unable to induce IL-1β secretion in these cells (Figure 1, B and C). Although LPS induced pro–IL-1β and pro–caspase-1 expression, CaOX crystals

Conflict of interest: The authors have declared that no conflict of interest exists.
Citation for this article: *J Clin Invest.* 2013;123(1):236–246. doi:10.1172/JCI63679.

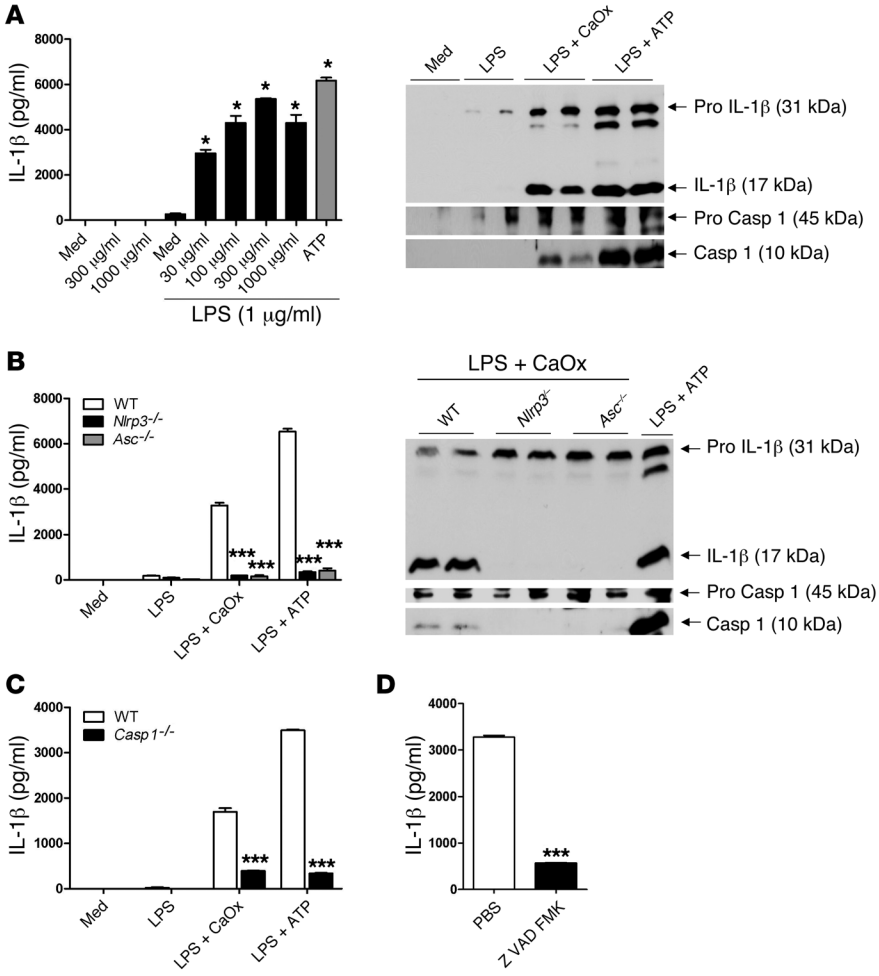

Figure 1
CaOx crystals activate DCs to secrete mature IL-1β. (**A**) WT BMDCs were stimulated with increasing doses of CaOx crystals with or without LPS prestimulation (1 μg/ml), and IL-1β secretion was measured by ELISA. ATP served as a positive control of NLRP3 activation. Western blotting of supernatants showed induction of pro–IL-1β by LPS; only CaOx crystals and ATP induced mature IL-1β secretion. This process involved caspase-1 activation (cleavage product, 10 kDa). (**B**) DCs from WT, *Nlrp3*$^{-/-}$, and *Asc*$^{-/-}$ mice. CaOx crystal– and ATP-induced IL-1β secretion depended on the presence of NLRP3 and ASC regardless of pro–IL-1β induction. (**C**) Similar results were obtained in DCs isolated from *Casp1*$^{-/-}$ mice. (**D**) WT BMDCs were stimulated with LPS/CaOx with or without the caspase inhibitor Z-VAD-FMK. Data are means ± SD from 3 separate experiments. **P* < 0.05 vs. medium; ****P* < 0.001 vs. respective WT (**B** and **C**) or PBS (**D**).

were unable to induce caspase-1 activation in *Nlrp3*$^{-/-}$, *Asc*$^{-/-}$, and *Casp1*$^{-/-}$ BMDCs, as was the case with LPS/ATP stimulation (Figure 1, B and C). Additionally, the caspase inhibitor Z-VAD-FMK had the same effect on LPS/CaOx crystal–induced IL-1β secretion in BMDCs (Figure 1D). Thus, CaOx crystals induced IL-1β secretion in DCs via the NLRP3/ASC/caspase-1 axis.

CaOx crystal–induced NLRP3 activation depends on phagocytosis and potassium efflux. Whether agonists directly interact with NLRP3 remains unknown, but various mechanisms are involved in NLRP3 activation by extracellular danger signals: particle uptake into the cell by phagocytosis, lysosomal cathepsin leakage, potassium efflux from the cell, P2X7 channel activation, and intracellular oxidative stress (15). We therefore performed a series of experiments to determine which of the aforementioned factors contributes to CaOx crystal–induced NLRP3 activation. Cytochalasin D, a phagocytosis-blocking agent that inhibited actin polymerization and crystal uptake into intracellular endosomes (Figure 2A), significantly reduced LPS/CaOx crystal–induced IL-1β secretion in BMDCs, whereas the cathepsin inhibitor CA074Me and the antioxidant N-acetyl cysteine had no effect (Figure 2B). Furthermore, blocking potassium efflux by a high concentration of potassium in the extracellular fluid had the same effect (Figure 2C), which suggests that potassium efflux is required for CaOx-induced NLRP3 activation. Comparison of LPS/CaOx crystal–induced IL-1β secretion between WT and *P2x7*$^{-/-}$ BMDCs did not support a contribution of P2X7 in this context (Figure 2D). Thus, CaOx crystals induced NLRP3-mediated IL-1β secretion in DCs via phagocytic uptake of CaOx crystals into intracellular endosomes as well as via inducing potassium efflux from the cell, a process known to activate NLRP3 (16).

CaOx crystals induce IL-1β secretion in renal DCs, but not in renal parenchymal cells. To determine whether CaOx crystals have a similar potential to activate renal DCs or renal parenchymal cells, we stimulated primary renal CD45^{+}CD11c^{+} DCs, ECs, mesangial cells (MCs), and tubular epithelial cells (TECs) with LPS/CaOx crystals as above. LPS/CaOx crystals induced IL-1β secretion in renal DCs in a manner similar to that of LPS/ATP, whereas none of the renal parenchymal cell types responded to the stimulation (Figure 2E). Western blotting confirmed this finding and also showed that LPS stimulation only induced pro–IL-1β expression in renal DCs (Figure 2F). Hence, CaOx crystals induced secretion of mature IL-1β only in renal DCs, not in renal parenchymal cells.

CaOx crystals induce ATP release from dying TECs. Consistent with previous reports (10), CaOx crystal exposure killed TECs (as demonstrated by lactate dehydrogenase [LDH] release) in a dose-dependent manner, independent of *Nlrp3* genotype (Supplemental Figure 3). Dying cells release intracellular damage-associated molecular pattern molecules (DAMPs) that have the potential to activate pattern recognition receptors of other cells (17). ATP is one such intracellular DAMP, reported to drive sterile inflamma-

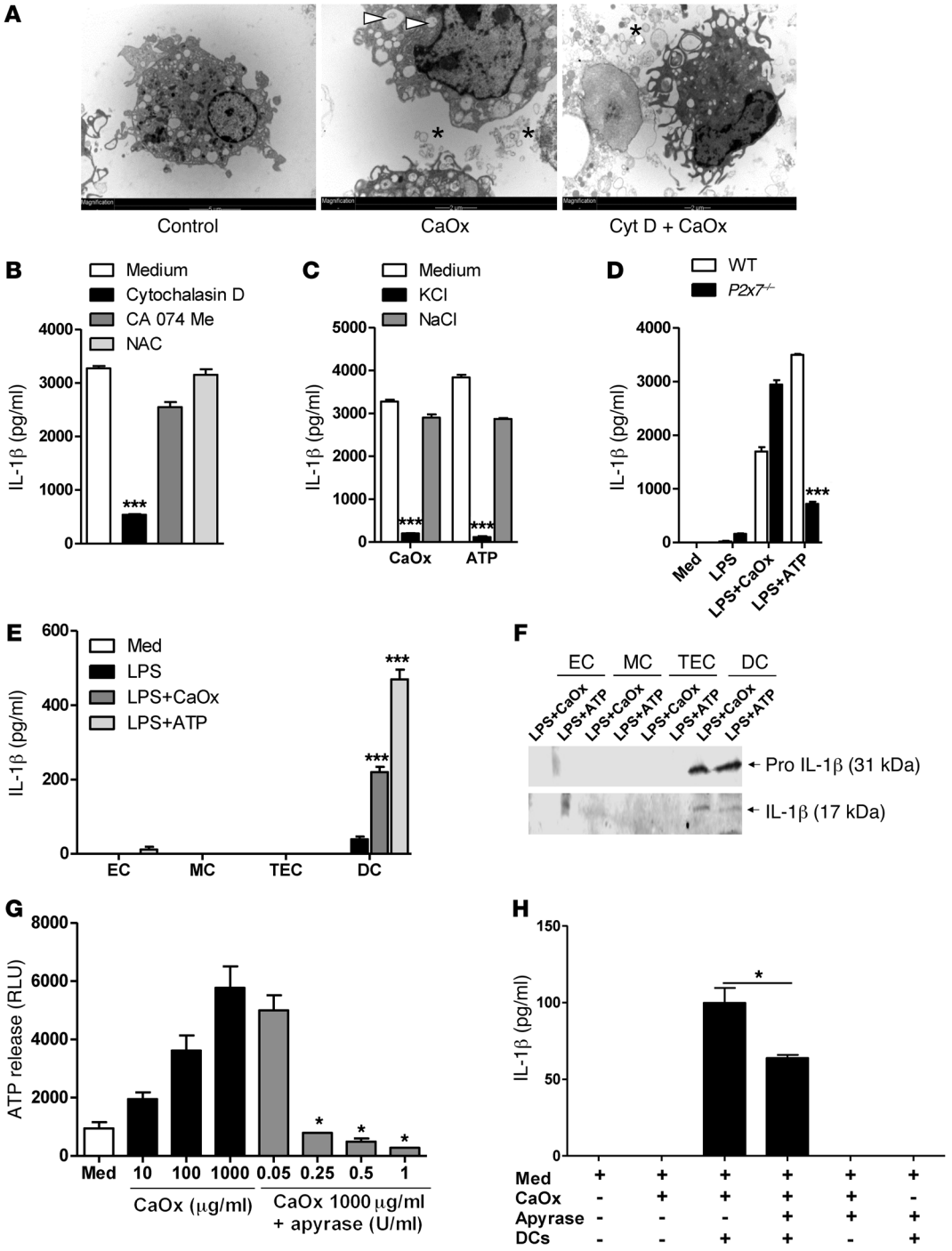

Figure 2

Mechanisms of CaOx crystal–induced IL-1β secretion. (**A**) BMDCs were primed with LPS (1 μg/ml) and stimulated with CaOx crystals in the presence or absence of cytochalasin D. TEM showed that CaOx crystals appeared outside the cell (asterisks) and inside intracellular endosomes (arrowheads), whereas cytochalasin D treatment inhibited their uptake in DCs. (**B**) Incubation with cytochalasin D, CA074Me, and N-acetyl cysteine (NAC) affected IL-1β secretion, measured by ELISA in cell culture supernatants after 6 hours. (**C**) Similar experiments were performed using 75 mM KCl in cell culture medium to block potassium efflux from the DCs. NaCl of an identical molarity was used as a molarity control. High extracellular potassium prevented CaOx-induced IL-1β secretion. (**D**) DCs were isolated from WT and *P2x7*$^{-/-}$ mice. ATP-induced, but not CaOx-induced, IL-1β secretion depended on the presence of P2X7. Data are means ± SD from 3 independent experiments. (**E**) Renal ECs, MCs, TECs, and renal DCs were primed with LPS and exposed to CaOx crystals, and IL-1β secretion was measured. ATP was used as a positive control for NLRP3 activation. (**F**) Western blotting. LPS priming induced pro–IL-1β expression only in DCs. (**G**) Primary TECs were isolated from WT mice and cultured with increasing concentrations of CaOx. ATP release was quantified in cell culture supernatant upon 18 hours of CaOx crystal exposure with and without increasing concentrations of apyrase. (**H**) Coculture of LPS-primed DCs with CaOx (100 μg/ml) damaged TECs with or without apyrase (1 U/ml). IL-1β secretion was measured by ELISA after 24 hours. Data are means ± SD from 3 independent experiments. **P* < 0.05, ***P* < 0.01, ****P* < 0.001 vs. medium (**B**, **C**, and **E**); vs. WT (**D**); vs. 1,000 μg/ml CaOx alone (**G**); or as indicated by brackets.

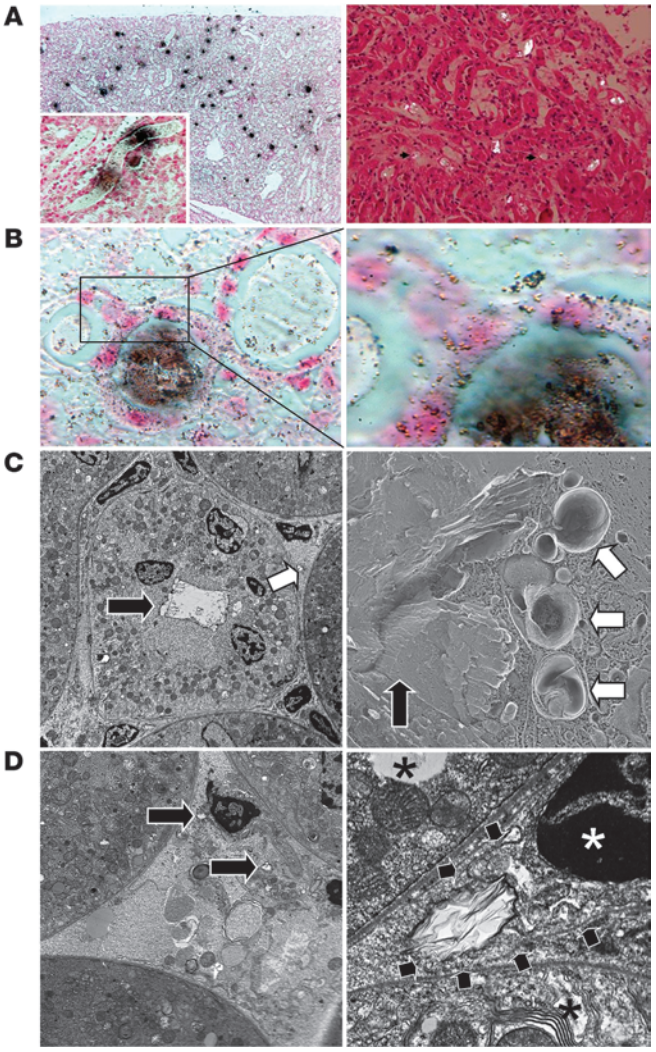

Figure 3
CaOx nephropathy in C57BL/6 mice. (**A**) Kidney sections showed CaOx crystals distributed throughout, especially in the tubular lumina (Pizzolato stain; left) or viewed under polarized light (right). Original magnification, ×100 (left); ×200 (right); ×400 (inset). (**B**) At higher magnification, Pizzolato stain showed smaller (granular) crystals inside TECs as well as in the renal interstitial compartment. Original magnification, ×400 (left), ×1,000 (right). (**C**) TEM (left) confirmed large CaOx crystal aggregates within the tubular lumen (black arrow) as well as in the interstitial space (white arrow). Freeze-fracture EM (right) identified CaOx crystals in the tubular lumen (black arrow) as well as inside cytoplasmic organelles, some of which appeared to be lysosomes (white arrows). Original magnification, ×3,000. (**D**) TEM also showed CaOx crystals within the interstitial compartment in close proximity to interstitial cells (left; black arrows). At higher magnification (right), an interstitial cell (white asterisk indicates nucleus) engulfed a CaOx crystal (black arrows denote outer cell membrane); neighboring TECs are denoted by black asterisks. Original magnification, ×7,000 (left); ×25,000 (right).

tion upon cell death via activation of NLRP3 (18, 19). Thus, we tested whether CaOx crystal–induced death of cultured TECs is associated with marked ATP release. In fact, CaOx crystal exposure induced ATP concentrations in cell culture supernatants in a dose-dependent manner (Figure 2G). In addition, extracellular ATP levels were readily degraded by adding apyrase at concentrations of 0.25 U/ml or higher (Figure 2G). Accordingly, coculture of BMDCs with CaOx-damaged primary tubular cells — with or without apyrase treatment — significantly reduced their capacity to secrete IL-1β (Figure 2H). Thus, CaOx crystals activated and destabilized TECs, a process that promoted the release of ATP, which activated DCs to release IL-1β.

Oxalate nephropathy involves diffuse crystal deposition, renal inflammation, and failure. Given the potential of CaOx crystals to activate renal DCs via NLRP3/ASC/caspase-1 in both direct and indirect ways, we suspected they make a functional contribution to oxalate nephropathy. Direct DC activation would require CaOx crystals to also reach the renal interstitial compartment, where DCs and other antigen-presenting cells span a dense network around the tubules (20). Murine oxalate nephropathy was characterized by diffuse CaOx crystal deposition throughout the kidney, with focal crystal casts obstructing proximal and distal tubules within the outer medulla as well as within the cortex, which was absent in control mice (Figure 3A and Supplemental Figure 4). Single crystals or small clumps of crystals, similar in appearance to the ones we applied for cell culture (Supplemental Figure 1), not only adhered to the luminal membranes of TECs, but were also found intracellularly within endosomes (Figure 3, B and C, and Supplemental Figure 5A). Diffuse CaOx crystal deposits were also found in the renal interstitial compartment, in close proximity to and within renal interstitial cells (Figure 3, B and D, and Supplemental Figure 5B). In fact, transmission EM (TEM) imaging showed that interstitial cells occasionally engulfed and took up crystals (Figure 3D). Renal CaOx crystal deposition was associated with diffuse neutrophil infiltrates and tubular necrosis mainly at the inner stripe of the outer medulla, as demonstrated by the disintegration of TECs and granular casts in tubular lumen (Figure 4, A and B). The structural alterations of oxalate nephropathy were associated with renal failure, as shown by a transient increase in plasma creatinine and BUN levels, peaking at 24 hours, compared with those in vehicle-injected mice (Figure 4A and Supplemental Figure 6). Intrarenal mRNA expression of the kidney injury markers KIM-1 and L-FABP, as well as that of the proinflammatory cytokines IL-6 and TNF-α, was increased (Figure 4C). Together, these observations indicated that murine oxalate nephropathy was characterized by diffuse CaOx crystal formation inside the tubular and the interstitial compartments, which is associated with tubular injury, renal inflammation, and failure.

Oxalate nephropathy depends on MyD88, IL-1R, and IL-18. Cytokine expression and neutrophil infiltration are suggestive of the involvement of innate immunity in oxalate nephropathy. To test this concept, we induced oxalate nephropathy in *Myd88*$^{-/-}$ mice, since MyD88 is a central signaling adaptor that translates innate pattern recognition into NF-κB activation and expression of proinflammatory cytokines, including pro–IL-1β and pro–IL-18 (21, 22). Unlike WT mice, *Myd88*$^{-/-}$ mice were almost entirely protected from acute kidney injury and failure, despite harboring identical CaOx crystal depositions (Figure 5). *Il1r*$^{-/-}$ mice were almost entirely protected, whereas *Il18*$^{-/-}$ mice displayed only partial protection (Figure 5). Thus, oxalate nephropathy depended on MyD88-mediated innate immunity, which also involved IL-1R and IL-18.

Oxalate nephropathy is abrogated in Nlrp3$^{-/-}$, *Asc*$^{-/-}$, *and Casp1*$^{-/-}$ *mice*. To test the functional contribution of the NLRP3/ASC/caspase-1 axis, we induced oxalate nephropathy in *Nlrp3*$^{-/-}$, *Asc*$^{-/-}$, or *Casp1*$^{-/-}$

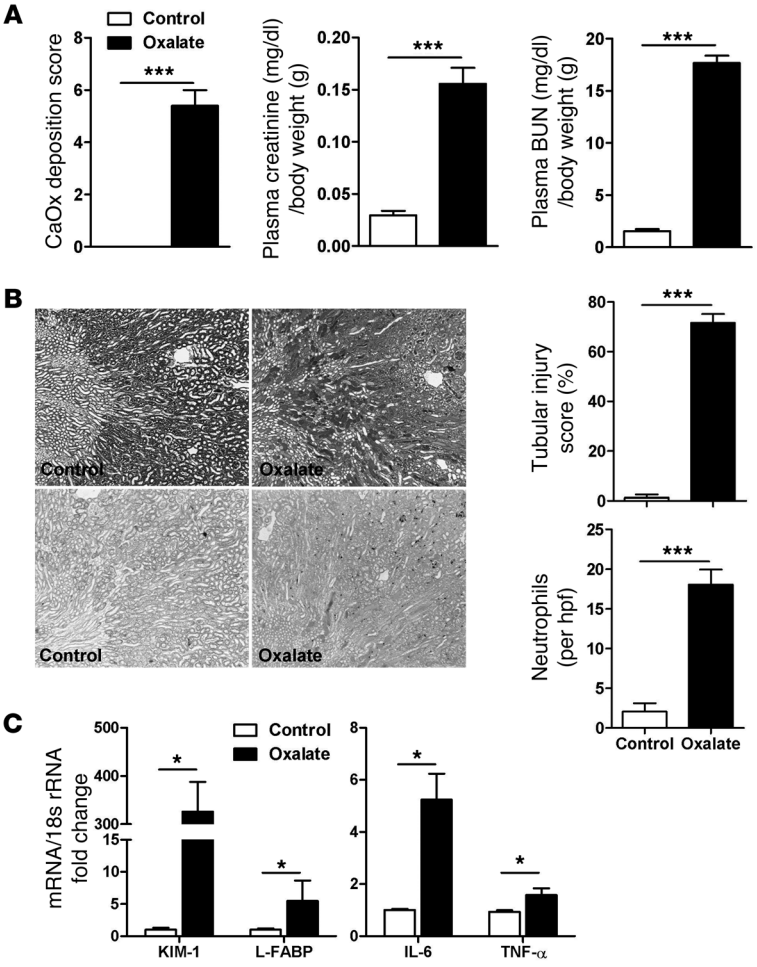

Figure 4

Oxalate nephropathy in C57BL/6 mice. (**A**) Oxalate feeding caused diffuse oxalate deposition within 24 hours and significantly increased plasma creatinine levels and BUN levels. (**B**) PAS staining illustrated tubular necrosis, which was quantified by semiquantitative scoring (loss of brush border, flattening of cells, disruption and detachment of tubular cells from basement membranes). Renal neutrophil counts were determined by Ly6G B1.2 immunostaining and quantified per 15 hpfs. Original magnification, ×100. (**C**) Renal mRNA expression was determined by real-time RT-PCR. Data are means ± SEM from 5–6 mice per group. $^{*}P < 0.05$, $^{***}P < 0.001$.

mice. Despite renal CaOx deposits identical to those of WT controls, all 3 groups were partially protected from kidney injury and failure, as evidenced by significant reductions in plasma creatinine, BUN, tubular damage, mRNA expression of tubular injury markers KIM-1 and L-FABP, and interstitial neutrophil infiltrates (Figure 6 and Supplemental Figure 7). Hence, NLRP3, ASC, and caspase-1 contributed to renal inflammation, damage, and dysfunction in CaOx nephropathy.

CaOx crystal–induced acute kidney injury depends on intrarenal mononuclear phagocytes. The results of our in vitro studies suggested that CaOx crystal–induced IL-1β secretion may selectively originate from the intrarenal network of mononuclear phagocytes, such as DCs and macrophages. Flow cytometry of renal cell suspension obtained after 24 hours of CaOx exposure revealed activation of $CD45^{+}CD11c^{+}$ intrarenal myeloid DCs, as evidenced by increased surface expression of CD40 and CD86 as well as by protrusions and dendrite expansion, visualized by scanning EM (Figure 7, A and B, and Supplemental Figure 8A). Next, we depleted monocytic phagocytes from the kidney by 2 injections of clodronate liposomes before inducing oxalate nephropathy. Depletion of $CD11c^{+}$ cells was confirmed by flow cytometry of renal cell suspensions (Supplemental Figure 8B). This procedure reduced intrarenal IL-1β production, as determined by ELISA from kidney homogenates (Supplemental Figure 8C). This was associated with partial protection from acute kidney injury compared with control liposome–treated mice (despite identical amounts of CaOx deposits), as documented by a significant reduction of plasma creatinine level, BUN level, and tubular damage (Figure 7C). Similar results were obtained when cells were selectively depleted by diphtheria toxin in CD11c DTRg mice (Figure 7D and Supplemental Figure 8, B and C). Thus, intrarenal mononuclear phagocytes mediated cytokine signaling and subsequent renal inflammation, injury, and failure in oxalate nephropathy.

Degradation of extracellular ATP with apyrase protects mice from oxalate nephropathy. Our in vitro studies showed that dying TECs released ATP, an endogenous NLRP3 agonist that triggers IL-1β secretion in DCs (19). Apyrase injection degrades extracellular ATP and can block the NLRP3-agonistic effect of this endogenous danger signal during sterile inflammation (18). We therefore used apyrase injections to test whether extracellular ATP also contributes to renal inflammation and injury during oxalate nephropathy. A single intraperitoneal injection of 20 U apyrase partially reduced tubular injury and neutrophil recruitment during oxalate nephropathy and improved renal excretory function, as documented by a significant reduction of plasma creatinine and BUN levels compared with vehicle-treated control mice (Figure 8A). Systemic IL-6 and MCP-1 levels were also reduced (Supplemental Figure 9A). We concluded that extracellular ATP (e.g., as it is released from dying TECs) served as an additional trigger for renal inflammation and dysfunction in oxalate nephropathy.

The recombinant IL-1R antagonist anakinra prevents oxalate nephropathy. All of the above observations suggested a functional role of NLRP3/ASC/caspase-1–mediated IL-1β secretion as a previously unrecognized pathomechanism for inflammation and tissue damage in CaOx nephropathy. Thus, therapeutic blockade of IL-1β may be able to interfere with this pathomechanism and protect against renal failure. Anakinra, a recombinant version of the endogenous IL-1 receptor antagonist, is approved by the FDA for the treatment of rheumatoid arthritis (23, 24). Intraperitoneal injection of anakinra dose-dependently reduced tubular injury and neutrophil recruitment and improved renal excretory function during oxalate nephropathy (Figure 8B and Supplemental Figure 9B). We concluded that IL-1β mediated inflammation and tissue damage in kidney injury induced by CaOx crystals, and thus IL-1 blockade protected from renal failure in oxalate nephropathy.

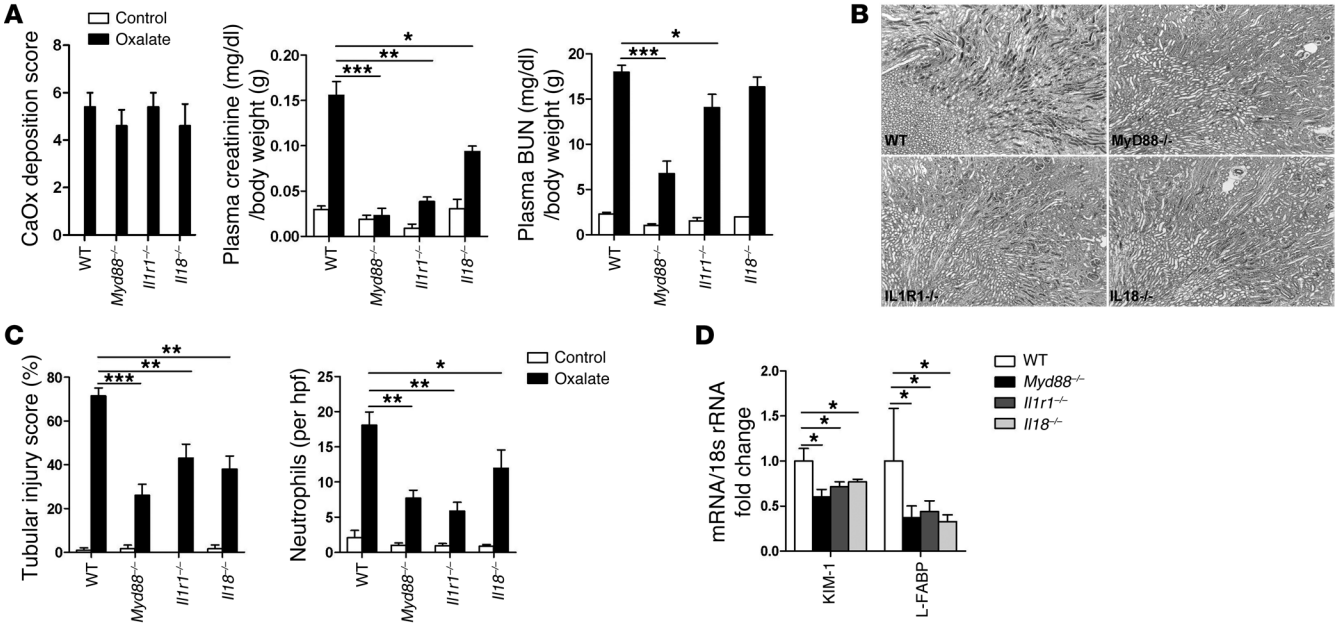

Figure 5

Role of MyD88, IL-1R, and IL-18 in CaOx nephropathy. (**A**) Oxalate deposition was similar in *Myd88*$^{-/-}$, *Il1r*$^{-/-}$, and *Il18*$^{-/-}$ mice, but plasma creatinine levels and BUN were not significantly increased, suggesting a protective role of these molecules in CaOX-induced renal damage. (**B**) PAS staining illustrated tubular necrosis. Original magnification, ×100. (**C**) Tubular injury score was determined by semiquantitative scoring, and renal neutrophil counts were determined by immunostaining and quantified per hpf. Data are means ± SEM from 5–6 mice per group. $^{*}P < 0.05$, $^{**}P < 0.01$, $^{***}P < 0.001$.

Discussion

Renal stone disease is widely considered to be a mechanical problem causing intra- or extrarenal urinary outflow obstruction, but crystal nephropathies are also associated with significant intrarenal inflammation that can cause acute kidney injury (3, 11). We hypothesized that the NLRP3 inflammasome — an intracellular pattern recognition platform that translates danger signaling into secretion of mature IL-1β — is involved in this process, because immune recognition of numerous crystals involves the NLRP3/ASC/caspase-1 axis (12–14).

In contrast to widely expressed Toll-like receptors or Rig-like helicases, the NLRP3/ASC/caspase-1 axis is restricted to antigen-presenting cells inside the kidney (25–27). We used clodronate liposome in WT mice or diphtheria toxin in CD11c DTRg mice to demonstrate that CaOx-induced intrarenal IL-1β secretion originated from the intrarenal network of interstitial mononuclear phagocytes, which includes several DC populations (28). CaOx crystals also formed in the interstitial compartment, where they were internalized by interstitial cells, a process demonstrated by us and others using TEM (present study and ref. 11). Our in vitro studies confirmed that phagocytic uptake was required for CaOx-induced IL-1β secretion in DCs, an observation consistent with the mode of NLRP3 activation by monosodium urate and calcium pyrophosphate crystals (12), silica (14), asbestos (14), and cholesterol crystals (13) in other disease contexts. Potassium efflux from the cell, occurring upon cell membrane disruption or pore formation by bacterial toxins, is another trigger of NLRP3 activation in DCs (15, 29). CaOx crystal–induced NLRP3 activation also depended on this mechanism, which was again consistent with previous reports on crystals of asbestos, monosodium urate (14), silica (30), cholesterol (31), and calcium phosphate (32). Intrarenal DCs and macrophages are important regulators of innate immunity and tissue remodeling in the kidney (28, 33). They express all known pattern recognition platforms that translate infectious and noninfectious dangers into local expression of proinflammatory cytokines and chemokines, causing subsequent immune-mediated pathology in the kidney (28, 33, 34). In addition, renal DCs express numerous negative regulators of innate immunity that limit overshooting renal inflammation and inappropriate kidney injury, e.g., in postischemic tubular necrosis (35–37). The present study is the first to our knowledge to demonstrate that acute kidney injury in crystal nephropathy largely depends on the capacity of intrarenal mononuclear phagocytes to trigger renal inflammation upon crystal recognition.

TEM and freeze-fracture EM demonstrated crystal uptake into intracellular compartments of TECs in vivo. TECs express NLRP3 but lack pro–IL-1β induction upon NF-κB priming (26, 38, 39). Therefore, CaOx crystals did not trigger mature IL-1β secretion in TECs. However, TECs internalize CaOx crystals, inducing oxidative stress and tubular cell necrosis (40–42). We confirmed this finding and showed that necrotic tubular cells released ATP, a potent NLRP3 agonist (19). Iyer et al. recently demonstrated that ATP is released upon acute tubular necrosis, which triggers NLRP3 activation and renal inflammation, a process that aggravates postischemic acute kidney injury (43). These results were supported by our present in vitro studies. In addition, the protective effects of apyrase treatment on CaOx nephropathy supported the functional contribution of ATP to renal inflammation and damage. It is noteworthy that apyrase injections also reduced plasma levels of IL-6 and MCP-1, implicating some systemic effects, which could be either causative or secondary for the improvement of the renal phenotype.

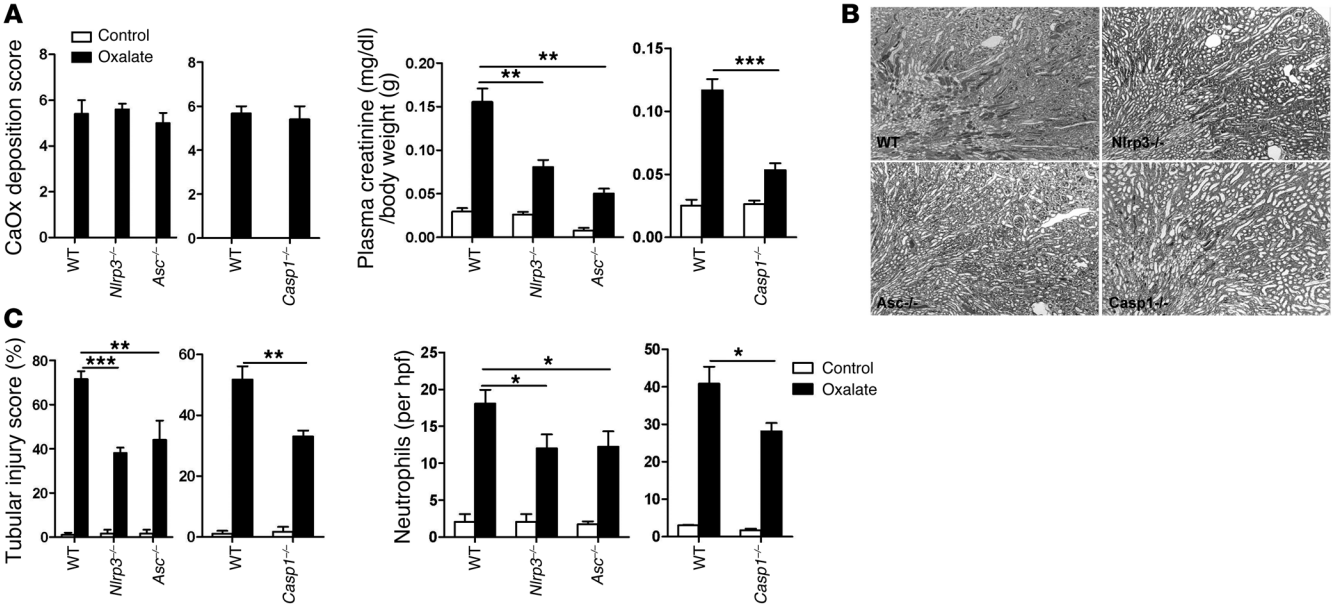

Figure 6
Role of NLRP3, ASC, and caspase-1 in CaOx nephropathy. (**A**) *Nlrp3*$^{-/-}$, *Asc*$^{-/-}$, and *Casp1*$^{-/-}$ mice showed CaOx deposits similar to those of WT mice, but decreased creatinine levels. (**B**) PAS staining illustrated reduced tubular necrosis compared with WT. Original magnification, ×100. (**C**) Tubular injury score and white cell counts were also reduced compared with WT. Data are means ± SEM from 5–6 mice per group. **P* < 0.05, ***P* < 0.01, ****P* < 0.001.

IL-1 blockade with appropriate antagonists is an established treatment of IL-1–dependent diseases, such as rheumatoid arthritis, Still's disease, and rare hereditary autoinflammatory disorders (24). Recently, IL-1 blockade also proved effective in crystal-mediated diseases, such as gout and pseudogout (44, 45). The dramatic therapeutic effects seem to directly relate to the fact that NLRP3 translates crystal recognition into IL-1β secretion as a central element of crystal-induced tissue inflammation and pathology (24). Our data demonstrated a similar therapeutic effect of the recombinant IL-1 receptor antagonist anakinra in CaOx nephropathy in mice, which suggests that IL-1 blockade may also reduce renal inflammation and kidney damage in other crystal nephropathies.

In conclusion, CaOx crystals triggered IL-1β–dependent innate immunity via the NLRP3/ASC/caspase-1 axis in DCs. Thus, intrarenal antigen-presenting cells promoted IL-1–dependent inflammation and kidney injury in renal stone disease. In addition, CaOx crystals indirectly activated NLRP3 by damaging TECs and releasing the NLRP3 agonist ATP. IL-1β blockade with anakinra prevented CaOx kidney injury disease, which could be a novel therapeutic approach to limit kidney damage in crystal nephropathies.

Methods

Animal studies

C57BL/6, NOD/ShiLt, NOD/*Casp1*$^{-/-}$, *Il1r1*$^{-/-}$, *Il18*$^{-/-}$, and *Myd88*$^{-/-}$ mice were procured from Jackson Laboratories. *Nlrp3*$^{-/-}$ and *Asc*$^{-/-}$ mice were provided by J. Tschopp (University of Lausanne, Lausanne, Switzerland) and by V. Dixit (Genentech, San Francisco, California, USA). CD11c DTRg mice were provided by C. Kurts (University of Bonn, Bonn, Germany) and D. Engel (University of Bonn, Bonn, Germany). Mice were housed in groups of 5 in filter top cages with unlimited access to food and water. Cages, food, and water were sterilized by autoclaving before use. 6- to 8-week-old mice received a single intraperitoneal injection of 100 mg/kg sodium oxalate and 3% sodium oxalate in drinking water, and kidneys were harvested after 24 hours. DC depletion was achieved by 2 intravenous injections of liposomal clodronate (200 μl) at 48 and 24 hours before injection of sodium oxalate. Control liposomes were used as vehicle control. In another experiment, CD11c DTRg mice were given a single intravenous injection of 8 ng diphtheria toxin (Sigma-Aldrich) 6 hours before sacrifice. Urine samples were collected after 24 hours, before sacrifice by cervical dislocation and harvest of plasma and kidney tissue (46). Kidneys were kept at –80°C for protein isolation and in RNA later solution at –20°C for RNA isolation. One part of the kidney was also kept in formalin to be embedded in paraffin for histological analysis.

Assessment of renal injury

Kidney sections (2 μm) were stained with periodic acid–Schiff (PAS) reagent. Tubular injury was scored by assessing the percentage of necrotic tubules and presence of tubular casts. Ly6B.2^{+} neutrophils were identified by immunostaining (clone 7/4; Serotec). Pizzolato staining visualized CaOx crystals, and crystal deposit formation in the kidney was evaluated as described previously (47), using the following point values: 0, no deposits; 1, crystals in papillary tip; 2, crystals in cortical medullary junction; 3, crystals in cortex. When crystals were observed in multiple areas, points were combined. Plasma creatinine and BUN were measured using Urea FS kit (DiaSys Diagnostic Systems) according to the manufacturer's protocol. Both parameters were corrected for body weight. Neutrophil infiltrates were counted in 15 high-power fields (hpfs) per section.

EM

Scanning EM. Kidney tissues were rinsed with PBS and postfixed with 1% aqueous osmium tetroxide for a total of 2.5 hours. Subsequently, tissues were rinsed and dehydrated through a graded series of ethanol to abso-

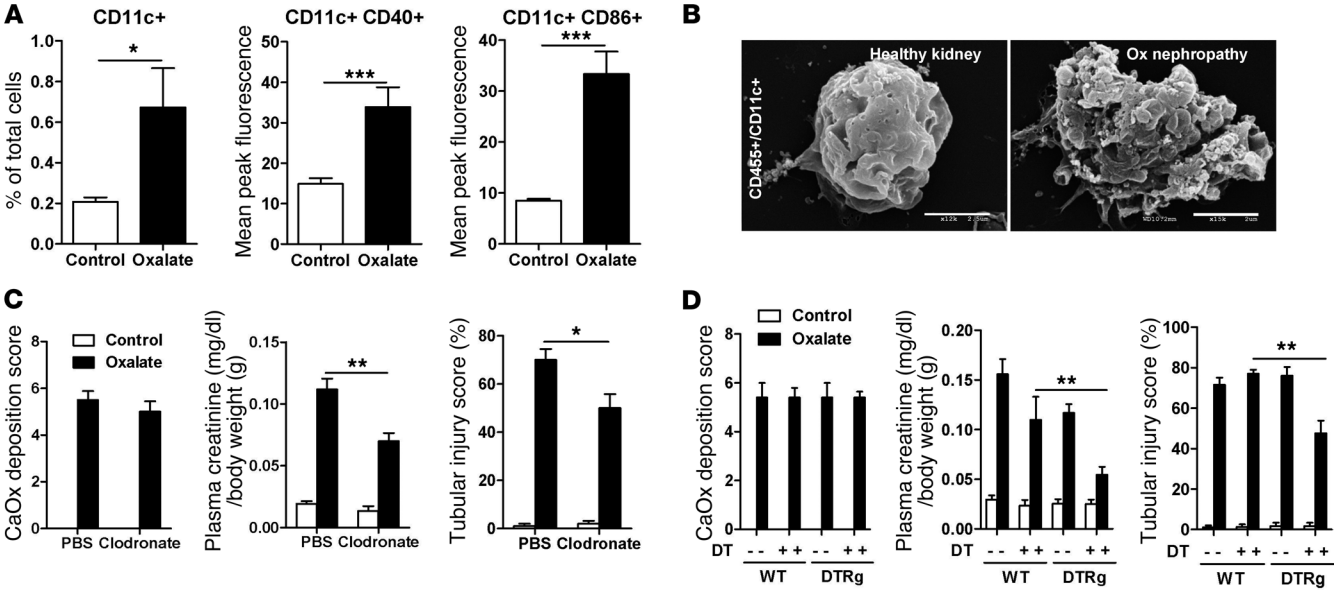

Figure 7

Role of DCs in CaOx nephropathy. $CD45^+CD11c^+$ cells were extracted from C57BL/6 by magnetic beads and sorted by flow cytometry using antibodies for the activation markers CD40 and MHC class II. (**A**) Percentage of cells with the specific markers. (**B**) $CD45^+CD11c^+$ cells were examined by scanning EM. DCs from CaOx mice showed marked cell surface disruption compared with the smooth bosselated surface of control cells. Scale bars: 2.5 μm. (**C**) CaOx nephropathy was induced in mice depleted of DCs (pretreated with clodronate liposomes) and compared with that in mice treated with control liposomes. (**D**) The same analyses were performed in CD11c DTRg mice in which $CD11c^+$ cells were depleted by diphtheria toxin (DT) injection. Data are means ± SEM from 5–6 mice per group. $^*P < 0.05$, $^{**}P < 0.01$, $^{***}P < 0.001$.

lute ethanol and critical-point dried using liquid CO_2. After mounting on stubs, the specimens were sputter-coated with a gold-palladium alloy for 1.5 minutes. DCs in suspension were rinsed in PBS and centrifuged to concentrate the cells. Then cells were dropped on coated coverslips and allowed to adhere; coverslips were fixed as above. Coverslips were cut into pieces prior to mounting on stubs. Images were viewed with a Hitachi 2600 electron microscope.

TEM. Kidneys were immersed in cold modified Karnovsky fixative containing 3% glutaraldehyde and 1% paraformaldehyde in sodium cacodylate buffer (pH 7.4) processed as previously described (48). In another set of experiments, BMDCs were stimulated with 1 μg/ml LPS and 100 μg/ml CaOx, with or without cytochalasin D pretreatment. After stimulation, cells were fixed with 2% paraformaldehyde with 2% glutaraldehyde in PBS buffer (pH 7.4) and processed. The samples were viewed with a JEOL model 1200EX electron microscope.

Quick-freeze deep-etch EM. 1.5-mm bread slices of nonfixed kidney or kidney sections fixed overnight in 2% glutaraldehyde in NaHCa (100 mM NaCl, 30 mM Hepes, and 2 mM $CaCl_2$, pH 7.2) were used after rinsing in NaHCa. Tissues were then cooled to 4°K with liquid helium; mounted in a Balzers 400 vacuum evaporator, fractured, and etched for 2.5 minutes at –104°C; rotary replicated with approximately 3 nm platinum, as previously described (49); and viewed using a JEOL 1400 microscope with attached AMT digital camera.

RNA preparation and real-time quantitative RT-PCR

Total RNA was isolated from kidneys using a Qiagen RNA extraction kit following the manufacturer's instructions. After quantification, RNA quality was assessed using agarose gels. From isolated RNA, cDNA was prepared using reverse transcriptase (Superscript II; Invitrogen). Real-time quantitative RT-PCR (TaqMan) was performed using SYBRGreen PCR master mix and analyzed with a Light Cycler 480 (Roche). All gene expression values were normalized using 18s RNA as a housekeeping gene. All primers used for amplification were from Metabion. The expression of KIM-1, IL-6, and TNF-α was analyzed using the following primers: Kim-1 forward, TCAGCTCGGGAATGCACA; Kim-1 reverse, TGGTTGCCTTCCGTGTCT; L-FABP forward, AGGCAATAGGTCTGCCCGAGGAC; L-FABP reverse, CCAGTTCGCACTCCTCCCCCA; IL-6 forward, TGATGCACTTGCAGAAAACA; IL-6 reverse, ACCAGAGGAAATTTTCAATAGGC; TNF-α forward, CCACCACGCTCTTCTGTCTAC; TNF-α reverse, AGGGTCTGGGCCATAGAACT.

Flow cytometry

Anti-mouse CD11c, CD40, CD86, and CD45 antibodies (BD Biosciences — Pharmingen) were used to detect activated DC and leukocyte populations in kidneys. F4/80, 7/4, and Ly6G antibodies (Abd Serotec) and CD3, NK1.1, CD11b, and CD103 antibodies (BD Biosciences — Pharmingen) were used to detect macrophage, neutrophil, T cell, natural killer cell, and mononuclear phagocyte populations in kidneys. Respective isotype antibodies were used to demonstrate specific staining of cell populations. Quantification of cell number was achieved using counting beads for FACS (Invitrogen).

Cell culture studies

BMDCs were established as described previously (50). Renal DCs were isolated from whole kidneys by magnetic bead separation (MACS) using CD11c MicroBeads (Miltenyi Biotech). The purity of $CD11c^+$ renal cells was confirmed by FACS analysis using anti-CD11c antibody (BD Biosciences — Pharmingen). Cells were stimulated for 3 hours with 1 μg/ml LPS followed by 100 μg/ml CaOx crystals or stimulated with 5 mM ATP for 6 hours (all Sigma-Aldrich). Cell-free supernatants were analyzed for cytokine secretion by ELISA (BD Biosciences — Pharmingen) and immunoblot analysis. Primary TECs were

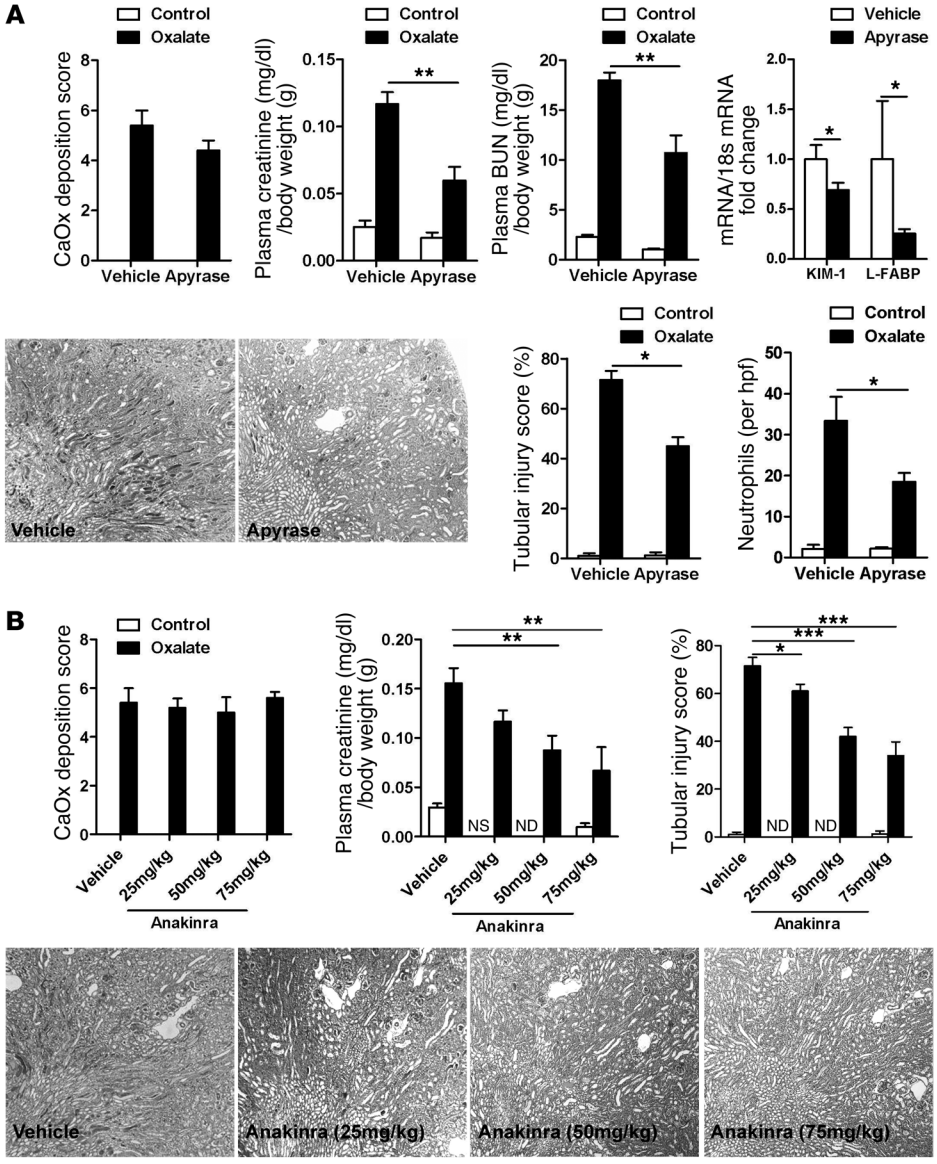

Figure 8
Apyrase and anakinra treatment in CaOx nephropathy in C57BL/6 mice. Oxalate nephropathy was induced in C57BL/6 mice treated with or without apyrase (**A**) and anakinra (**B**), and oxalate deposition was quantified using Pizzolato stains. Plasma creatinine levels were determined as described in Methods. Tubular injury score was determined by semiquantitative scoring of PAS sections, and renal neutrophil counts were determined by immunostaining and quantified per hpf. Original magnification, ×100. Data are means ± SEM from 5–6 mice per group. $^{*}P < 0.05$, $^{**}P < 0.01$, $^{***}P < 0.001$. ND, not done.

isolated from the kidneys and grown on type IV collagen–coated tissue culture plates (Sigma-Aldrich). Primary renal ECs and MCs were isolated as described previously (26). The isolated primary cells were confirmed under light microscope and further characterized by FACS, immunostaining, Western blot, and RT-PCR. Cells were grown to confluency before use. 1×10^5 cells per well were used. Primary TECs were maintained in DMEM/F12 (Sigma-Aldrich) containing 10% FCS (Sigma-Aldrich), 1% penicillin-streptomycin (Sigma-Aldrich), 125 ng/ml prostaglandin E1 (Calbiochem), 25 ng/ml EGF (Sigma-Aldrich), 1.8 μg/ml L-thyroxine (Sigma-Aldrich), 3.38 ng/ml hydrocortisone (Sigma-Aldrich), and 2.5 mg/ml insulin–transferrin–sodium selenite supplement (I-T-SS; Sigma-Aldrich). Primary endothelia and MCs were maintained in DMEM (Gibco, Invitrogen) plus 10% FCS and 1% penicillin-streptomycin, and primary renal DCs were maintained in RPMI (Gibco, Invitrogen) and used immediately. All cells were cultured in an incubator at 37°C, 5% CO_2. Supernatants were analyzed for LDH release using the CytoTox 96 Non-Radioactive Cytotoxicity Assay Kit (Promega) to evaluate cell death, measuring LDH after 18 hours. Results were expressed as percent of positive control. For ATP release, the system bioluminescence detection kit for ATP measurement was used (Promega), following the manufacturer's instructions.

Coculture studies

Briefly, TECs and BMDCs were generated as described above. TECs were treated with or without 100 μg/ml CaOx for 18 hours, after which the supernatants were treated with 1 U/ml apyrase (Sigma-Aldrich). Next, LPS-primed (1 μg/ml) or unprimed BMDCs were cocultured with the TECs at a 4:1 ratio in RPMI 1640 (Gibco, Invitrogen) supplemented with 10% FBS. After 24 hours of coculture, the supernatants were collected, centrifuged, and analyzed for IL-1β concentration by ELISA (BD Biosciences — Pharmingen).

Immunoblots

Upon completion of the 6-hour stimulation experiment, supernatants and cells were collected. Supernatants were concentrated using Amicon Ultra centrifugal filters (Millipore Billerica) and resolved on 15% SDS polyacryl-

amide gels. After electrophoresis, proteins were transferred to PVDF membrane. Primary antibodies were goat polyclonal anti–IL-1β (BAF401; R&D Systems) and rabbit polyclonal anti–caspase-1 (sc-514; Santa Cruz); this was followed by incubation with secondary antibody anti-biotin or anti-rabbit IgG labeled with HRP. Immunostained bands were detected using a chemiluminescence kit (ECL kit).

Statistics

Data are presented as mean ± SEM. Comparison of groups was performed using ANOVA; post-hoc Bonferroni correction was used for multiple comparisons. A P value less than 0.05 was considered significant.

Study approval

All experimental procedures were approved by the local government authorities.

Acknowledgments

The study was funded by the Deutsche Forschungsgemeinschaft (GRK 1202 and AN372/9-2). The expert technical support of Heni Eka Susanti, Dan Draganovici, Nuru Eltrich, and Jana Mandelbaum is acknowledged, as is the expert technical support of Jaclyn Lett (WUSTL Research Core Lab for Auditory and Vestibular Studies, funded by NIH/NIDCD grant no. P30DC04665 SEM), Karen Green (Pathology and Immunology Electron Microscopy Research Core lab, Washington University School of Medicine), and Robyn Roth (Heuser Lab, Department of Cell Biology, Washington University School of Medicine). We thank Christian Kurts and Daniel Engel for providing CD11c DTRg mice.

Received for publication March 2, 2012, and accepted in revised form October 11, 2012.

Address correspondence to: Hans-Joachim Anders, Medizinische Klinik und Poliklinik IV, Klinikum der Universität München, Ziemssenstr. 1, 80336 München, Germany. Phone: 49.89.218075855; Fax: 49.89.218075860; E-mail: hjanders@med.uni-muenchen.de.

1. Pearle MS, Calhoun EA, Curhan GC. Urologic diseases in America project: urolithiasis. *J Urol*. 2005;173(3):848–857.
2. Evan AP, et al. Renal histopathology and crystal deposits in patients with small bowel resection and calcium oxalate stone disease. *Kidney Int*. 2010;78(3):310–317.
3. Rule AD, Krambeck AE, Lieske JC. Chronic kidney disease in kidney stone formers. *Clin J Am Soc Nephrol*. 2011;6(8):2069–2075.
4. Hoppe B, Beck BB, Milliner DS. The primary hyperoxalurias. *Kidney Int*. 2009;75(12):1264–1271.
5. Robijn S, Hoppe B, Vervaet BA, D'Haese PC, Verhulst A. Hyperoxaluria: a gut-kidney axis? *Kidney Int*. 2011;80(11):1146–1158.
6. McMartin K. Are calcium oxalate crystals involved in the mechanism of acute renal failure in ethylene glycol poisoning? *Clin Toxicol (Phila)*. 2009; 47(9):859–869.
7. Evan AP. Physiopathology and etiology of stone formation in the kidney and the urinary tract. *Pediatr Nephrol*. 2010;25(5):831–841.
8. Okada A, et al. Genome-wide analysis of genes related to kidney stone formation and elimination in the calcium oxalate nephrolithiasis model mouse: detection of stone-preventive factors and involvement of macrophage activity. *J Bone Miner Res*. 2009;24(5):908–924.
9. Katsuma S, et al. Global analysis of differentially expressed genes during progression of calcium oxalate nephrolithiasis. *Biochem Biophys Res Commun*. 2002;296(3):544–552.
10. Khan SR. Crystal-induced inflammation of the kidneys: results from human studies, animal models, and tissue-culture studies. *Clin Exp Nephrol*. 2004;8(2):75–88.
11. Okada A, et al. Renal macrophage migration and crystal phagocytosis via inflammatory-related gene expression during kidney stone formation and elimination in mice: Detection by association analysis of stone-related gene expression and microstructural observation. *J Bone Miner Res*. 2010; 25(12):2701–2711.
12. Martinon F, Petrilli V, Mayor A, Tardivel A, Tschopp J. Gout-associated uric acid crystals activate the NALP3 inflammasome. *Nature*. 2006; 440(7081):237–241.
13. Duewell P, et al. NLRP3 inflammasomes are required for atherogenesis and activated by cholesterol crystals. *Nature*. 2010;464(7293):1357–1361.
14. Dostert C, Petrilli V, Van Bruggen R, Steele C, Mossman BT, Tschopp J. Innate immune activation through Nalp3 inflammasome sensing of asbestos and silica. *Science*. 2008;320(5876):674–677.
15. Schroder K, Tschopp J. The inflammasomes. *Cell*. 2010;140(6):821–832.
16. Petrilli V, Papin S, Dostert C, Mayor A, Martinon F, Tschopp J. Activation of the NALP3 inflammasome is triggered by low intracellular potassium concentration. *Cell Death Differ*. 2007;14(9):1583–1589.
17. Kono H, Rock KL. How dying cells alert the immune system to danger. *Nat Rev Immunol*. 2008; 8(4):279–289.
18. McDonald B, et al. Intravascular danger signals guide neutrophils to sites of sterile inflammation. *Science*. 2010;330(6002):362–366.
19. Mariathasan S, et al. Cryopyrin activates the inflammasome in response to toxins and ATP. *Nature*. 2006;440(7081):228–232.
20. Soos TJ, et al. CX(3)CR1(+) interstitial dendritic cells form a contiguous network throughout the entire kidney. *Kidney Int*. 2006;70(3):591–596.
21. Muzio M, Ni J, Feng P, Dixit VM. IRAK (Pelle) family member IRAK-2 and MyD88 as proximal mediators of IL-1 signaling. *Science*. 1997;278(5343):1612–1615.
22. Medzhitov R, et al. MyD88 is an adaptor protein in the hToll/IL-1 receptor family signaling pathways. *Mol Cell*. 1998;2(2):253–258.
23. Mertens M, Singh JA. Anakinra for rheumatoid arthritis. *Cochrane Database Syst Rev:CD*. 2009;2009:Rev:CD005121.
24. Dinarello CA. Interleukin-1beta and the autoinflammatory diseases. *N Engl J Med*. 2009; 360(23):2467–2470.
25. Anders HJ. Toll-like receptors and danger signaling in kidney injury. *J Am Soc Nephrol*. 2010; 21(8):1270–1274.
26. Lichtnekert J, et al. Anti-GBM glomerulonephritis involves IL-1 but is independent of NLRP3/ASC inflammasome-mediated activation of caspase-1. *PLoS One*. 2011;6(10):e26778.
27. Ribeiro A, et al. Activation of innate immune defense mechanisms contributes to polyomavirus BK-associated nephropathy. *Kidney Int*. 2012;81(1):100–111.
28. Nelson PJ, Rees AJ, Griffin MD, Hughes J, Kurts C, Duffield J. The renal mononuclear phagocytic system. *J Am Soc Nephrol*. 2012;23(2):194–203.
29. Allam R, Darisipudi MN, Rupanagudi KV, Lichtnekert J, Tschopp J, Anders HJ. Cutting edge: cyclic polypeptide and aminoglycoside antibiotics trigger IL-1beta secretion by activating the NLRP3 inflammasome. *J Immunol*. 2011;186(5):2714–2718.
30. Cassel SL, et al. The Nalp3 inflammasome is essential for the development of silicosis. *Proc Natl Acad Sci U S A*. 2008;105(26):9035–9040.
31. Rajamaki K, et al. Cholesterol crystals activate the NLRP3 inflammasome in human macrophages: a novel link between cholesterol metabolism and inflammation. *PLoS One*. 2010;5(7):e11765.
32. Pazar B, et al. Basic calcium phosphate crystals induce monocyte/macrophage IL-1beta secretion through the NLRP3 inflammasome in vitro. *J Immunol*. 2011;186(4):2495–2502.
33. Anders HJ, Ryu M. Renal microenvironments and macrophage phenotypes determine progression or resolution of inflammation and fibrosis. *Kidney Int*. 2011;80(9):915–925.
34. Anders HJ, Muruve DA. The inflammasomes in kidney disease. *J Am Soc Nephrol*. 2011;22(6):1007–1018.
35. Lech M, et al. Resident dendritic cells prevent postischemic acute renal failure by help of single Ig IL-1 receptor-related protein. *J Immunol*. 2009;183(6):4109–4118.
36. Lassen S, Lech M, Rommele C, Mittruecker HW, Mak TW, Anders HJ. Ischemia reperfusion induces IFN regulatory factor 4 in renal dendritic cells, which suppresses postischemic inflammation and prevents acute renal failure. *J Immunol*. 2010;185(3):1976–1983.
37. Lech M, et al. Oxidative stress stimulates renal dendritic cells to secrete pentraxin-3 which limits acute kidney injury by inhibiting neutrophil and macrophage recruitment. *Kidney Int*. In press.
38. Shigeoka AA, et al. An inflammasome-independent role for epithelial-expressed Nlrp3 in renal ischemia-reperfusion injury. *J Immunol*. 2010;185(10):6277–6285.
39. Vilaysane A, et al. The NLRP3 inflammasome promotes renal inflammation and contributes to CKD. *J Am Soc Nephrol*. 2010;21(10):1732–1744.
40. Schepers MS, van Ballegooijen ES, Bangma CH, Verkoelen CF. Crystals cause acute necrotic cell death in renal proximal tubule cells, but not in collecting tubule cells. *Kidney Int*. 2005;68(4):1543–1553.
41. Khan SR. Role of renal epithelial cells in the initiation of calcium oxalate stones. *Nephron Exp Nephrol*. 2004;98(2):e55–e60.
42. Knoll T, et al. The influence of oxalate on renal epithelial and interstitial cells. *Urol Res*. 2004; 32(4):304–309.
43. Iyer SS, et al. Necrotic cells trigger a sterile inflammatory response through the Nlrp3 inflammasome. *Proc Natl Acad Sci U S A*. 2009;106(48):20388–20393.
44. So A, et al. Canakinumab for the treatment of acute flares in difficult-to-treat gouty arthritis: Results of

a multicenter, phase II, dose-ranging study. *Arthritis Rheum*. 2010;62(10):3064–3076.
45. McGonagle D, Tan AL, Madden J, Emery P, McDermott MF. Successful treatment of resistant pseudogout with anakinra. *Arthritis Rheum*. 2008;58(2):631–633.
46. Ninichuk V, et al. The role of interstitial macrophages in nephropathy of type 2 diabetic db/db mice. *Am J Pathol*. 2007;170(4):1267–1276.
47. Yamaguchi S, Wiessner JH, Hasegawa AT, Hung LY, Mandel GS, Mandel NS. Study of a rat model for calcium oxalate crystal formation without severe renal damage in selected conditions. *Int J Urol*. 2005;12(3):290–298.
48. Schmidt RE, Parvin CA, Green KG. Synaptic ultrastructural alterations anticipate the development of neuroaxonal dystrophy in sympathetic ganglia of aged and diabetic mice. *J Neuropathol Exp Neurol*. 2008;67(12):1166–1186.
49. Heuser J. Preparing biological samples for stereomicroscopy by the quick-freeze, deep-etch, rotary-replication technique. *Methods Cell Biol*. 1981; 22:97–122.
50. Darisipudi MN, Allam R, Rupanagudi KV, Anders HJ. Polyene macrolide antifungal drugs trigger interleukin-1beta secretion by activating the NLRP3 inflammasome. *PLoS One*. 2011;6(5):e19588.